



ELSEVIER

15 September 2001

OPTICS  
COMMUNICATIONS

Optics Communications 197 (2001) 201–207

www.elsevier.com/locate/optcom

# Electro-optically controlled beam deflection for grazing incidence geometry on a domain-engineered interface in $\text{LiNbO}_3$

Robert W. Eason <sup>\*</sup>, Alexander J. Boyland, Sakellaris Mailis, Peter G.R. Smith

*Optoelectronics Research Centre, University of Southampton, Southampton SO17 1BJ, UK*

Received 10 April 2001; accepted 9 July 2001

## Abstract

We report an analysis on the electro-optically induced beam deflection experienced by light traversing an interface between two anti-parallel domains in a sample of  $\text{LiNbO}_3$ . In contrast to other work on prism deflection schemes, we present a grazing incidence geometry for light at incidence angles between  $87.7^\circ$  and  $89.0^\circ$  that has been investigated to maximise the deflection angles achievable. Further improvements can be obtained for both range of angular deflection and transmission uniformity, by faceting the exit face of the device at an optimum angle. We present a theoretical analysis for this configuration and compare with data obtained for a wavelength of  $1.52 \mu\text{m}$ . A practical geometry would permit a deflection of  $\sim 140$  mrad for an applied voltage of 1 kV. © 2001 Elsevier Science B.V. All rights reserved.

*Keywords:* Lithium niobate; Electro-optic effect; Domain engineering; Beam scanning; Beam deflection

## 1. Introduction

Solid-state devices developed for beam scanning and deflection have been widely reported in the recent past. Requirements of speed, compactness and integration have favoured the use of domain-engineered samples of ferroelectrics such as  $\text{LiNbO}_3$  and  $\text{LiTaO}_3$  that permit electro-optic control of local refractive index, thereby enabling small changes in propagation direction via refraction at an interface. Prism type geometries are perhaps the most reported to date, in which light is incident on a series of triangular domain-inverted

regions, the deflection angles achievable being a function of both geometry and number of prisms [1,2]. Further levels of integration have also been reported, in which scanning has been integrated with focussing elements [3], second harmonic generation [4], and for use as a laser Q-switch [5].

Although recent work has addressed the problem of optimising the design of such electro-optic prism scanners, and also discussed the alternative gradient index deflectors, where the light ray is bent as it propagates through a region of non-uniform refractive index [6], there remains a fundamental problem with this approach. The linear electro-optic effect in  $\text{LiNbO}_3$  or  $\text{LiTaO}_3$  is comparatively weak, and at moderate field strengths of  $\sim 1 \text{ kV mm}^{-1}$ , the deflection angles achievable are small. As an illustration of this limitation, we show

<sup>\*</sup> Corresponding author. Tel.: +44-23-80592098; fax: +44-23-80593142.

*E-mail address:* rwe@orc.soton.ac.uk (R.W. Eason).

below calculations of deflection angle,  $\delta$ , achieved for a single e–o prism deflector under four different electric field addressing geometries.

The equation relating the induced refractive index change,  $\Delta n$ , under electro-optic addressing, as a function of electric field strength  $E_z$  is given by the usual expression below:

$$\Delta n = -(1/2)r_{33}n_e^3E_z \quad (1)$$

where  $r_{33}$  is the largest electro-optic coefficient accessed by extraordinary polarised light,  $n_e$  is the wavelength dependent value of extraordinary refractive index, and  $E_z$  is the electric field strength applied across the sample in the  $z$ -direction.

For simplicity, and as a means of comparison between existing electro-optic prism designs and our near total internal reflection (TIR) geometry, we standardise on a common set of values for refractive index, electro-optic coefficient, and value of applied electric field strength. These are:  $n_e = 2.23$ ,  $r_{33} = 30.8 \times 10^{-12} \text{ mV}^{-1}$ , and  $E_z = 1 \text{ kV mm}^{-1}$  ( $10^6 \text{ V m}^{-1}$ ), which relate to congruent single crystal  $\text{LiNbO}_3$  for light in the mid-visible region of the spectrum at  $\sim 550 \text{ nm}$ . Shown in Fig. 1 is the familiar geometry for beam deflection via a prism of apex angle  $\alpha$ . For electro-optic addressing there are four possible conditions for producing beam deflection when an electric field is applied to either the prism and/or the background host material. Values of deflection angle may be increased by a factor of two by simultaneously increasing one refractive index (e.g.  $n_2$ ), while reducing the other ( $n_1$ ) by the same amount, as is the case for a

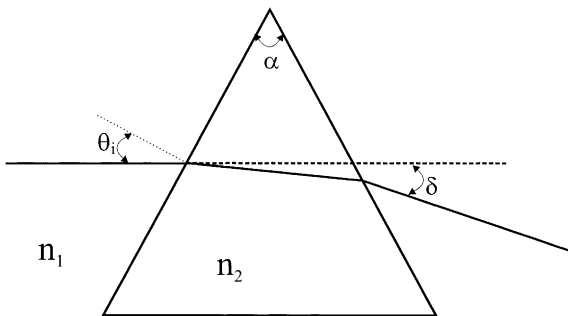


Fig. 1. Schematic of refraction through a prism of refractive index  $n_2$  in a host medium of index  $n_1$ . Overall angular deflection is  $\delta$ .

Table 1

Four combinations of indices  $n_1$  and  $n_2$  for electro-optic addressing of prism and/or host material, and resultant values of  $n_{21}$  and associated value of  $\delta$

$n_1$	$n_2$	$n_{21} = n_2/n_1$	$\delta/\text{deg}$
$n - \Delta n$	$n + \Delta n$	1.000153	0.010
$n$	$n + \Delta n$	1.000077	0.005
$n + \Delta n$	$n - \Delta n$	0.999849	-0.005
$n$	$n - \Delta n$	0.999923	-0.010

uniform field applied to a domain inverted sample. Additionally, as has been demonstrated in Ref. [3] for example, prisms can be cascaded so that the achievable deflection angles are increased as a linear function of the number of prisms. Finally, as the beam emerges into air from a medium of refractive index  $\sim 2.2$ , there is a final magnification of the deflection achieved by this same factor, in the small deflection limit.

Table 1 shows the calculated values of beam deflection angle for these four different geometries, for a common angle of incidence of  $30^\circ$ , at an applied electric field of  $1 \text{ kV mm}^{-1}$ . Of note here are the small values obtained for  $\delta$ , which have been calculated for a single prism of apex angle  $60^\circ$ , for the four possible combinations of  $n_2/n_1$ , which we abbreviate to  $n_{21}$ . Even for the most favourable case where  $n_1 = n - \Delta n$ , and  $n_2 = n + \Delta n$ , the deflection angle achieved is only  $0.01^\circ$ . In Ref. [3], where seven prisms are used in series, and the applied field was  $\sim 4.4 \text{ kV mm}^{-1}$ , this produces a total deflection angle of  $\sim 0.3^\circ$ , which is magnified to  $\sim 0.66^\circ$  when the beam is refracted into the air. In Ref. [3] where  $\alpha$  was of order  $66^\circ$ , the reported beam deflection was  $0.72^\circ$  (12.65 mrad).

Fig. 2 shows exact calculations of deflection angle  $\delta$  for the four possible electro-optic geometries, using the following equation for beam deflection via a prism of apex angle  $\alpha$  [7]:

$$\delta = \theta_i - \alpha + \sin^{-1} \left\{ \sin \alpha [(n_{21})^2 - \sin^2 \theta_i]^{1/2} - \sin \theta_i \cos \alpha \right\} \quad (2)$$

where  $\theta_i$  is the angle of incidence. As expected the plots are symmetrical about the zero deflection line, but what is immediately apparent is that the  $\sim 30^\circ$  angles typically used for  $\theta_i$  in prism scanners

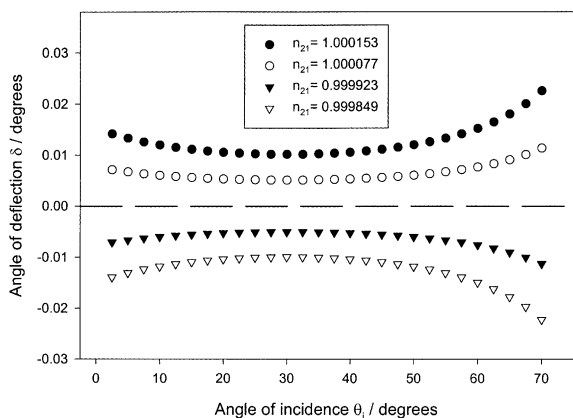


Fig. 2. Angle of deflection  $\delta$  as a function of angle of incidence  $\theta_i$  for  $n_{21}$  values as shown in Table 1.

represents the precise angle for which minimum deviation is produced. This choice of angle is necessary however when cascaded prisms are used as in Ref. [3], and in-line prism fabrication is the preferred route.

It is therefore apparent that the single prism deflection result of  $\sim 0.01^\circ$  for a normalised value of applied electric field of  $1 \text{ kV mm}^{-1}$  may be increased if alternative geometries are adopted. This paper discusses the use of a near TIR geometry, which we have already successfully used to demonstrate a switch with a measured contrast ratio exceeding 100:1 [8]. In this implementation however, it is the deflection of the transmitted beam we are considering, rather than the switching into TIR.

## 2. TIR beam deflection geometry

The first reference to our knowledge concerning such TIR switching geometries was reported in connection with bulk Bragg grating structures in  $\text{LiNbO}_3$  [9], where the authors reported switching efficiencies of up to 95%. For the geometry reported in this paper however, we consider only a single interface region. Fig. 3 shows a schematic of

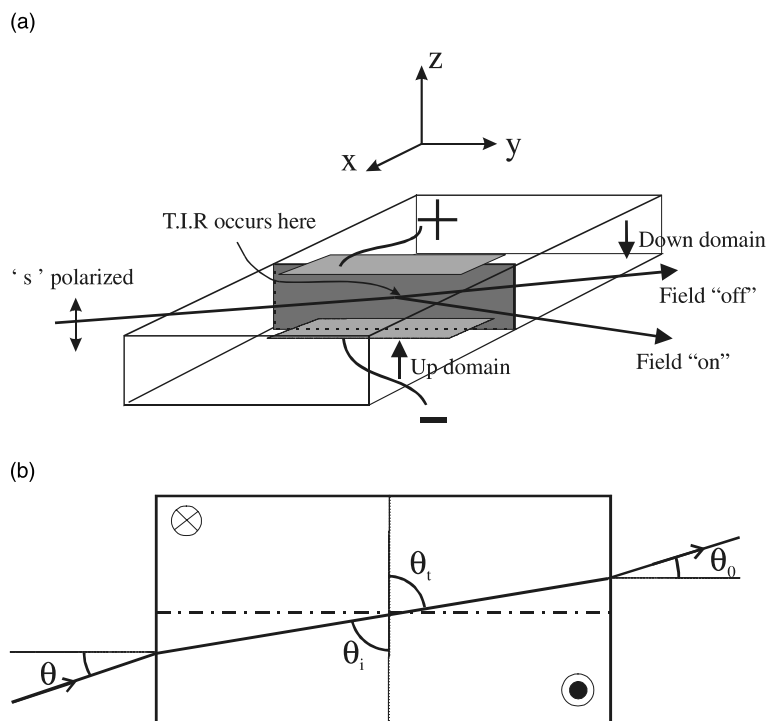


Fig. 3. (a) Schematic of domain engineered sample used for beam scanning. Input light is 's' polarised. (b) Plan view of scanner showing angles referred to in the text.

the electro-optic TIR geometry for a domain engineered LiNbO<sub>3</sub> switch/scanner. The sample was a 300 μm thick z-cut congruent LiNbO<sub>3</sub> wafer supplied by Yamaju (Japan), with dimensions in the *x* and *y* directions of 13.5 mm × 15 mm. The *-z* face was photolithographically patterned and electric field poled to produce a structure consisting of two anti-parallel domains. Under polarised light microscopic examination, the interface layer was seen to be quite flat and smooth, but some fine detail, including local variation from absolute straightness was observed in all the engineered samples produced. After poling, annealing was performed at 200°C for several hours, to attempt to remove any residual strain at the interface. Experiments performed for TIR switching however revealed that even after annealing a small residual refractive index existed across this interface which was of order 10<sup>-5</sup> [8].

Experiments were performed using the two laser wavelengths of 0.543 and 1.523 μm from separate polarised He–Ne laser sources, both of output power ~ 0.6 mW. Focussing into the LiNbO<sub>3</sub> sample was achieved by a lens of focal length 160 mm, which produced a spot size of order 25 μm for the 0.543 μm light. Electrodes were fabricated on both + and *-z* faces, of dimensions ~ 12 mm × 2 mm, across the domain interface region. The input and exit faces were parallel polished, and the device was mounted on an insulating support.

Before characterising the scanner performance, simulations were run based on the change of the refracted ray direction at the electro-optically addressed interface. Unlike the case for electro-optic prism scanning, the grazing incidence geometry is uniquely sensitive to small changes of local index. Applying Snell's law to the interface yields:

$$(n + \Delta n) \sin \theta_i = (n - \Delta n) \sin \theta_t \quad (3)$$

where  $\Delta n$  is as defined in Eq. (1).

Fig. 4 shows values of  $\theta_t$  calculated via Eq. (3), as a function of voltage applied across the interface, for values of  $\theta_i$  ranging from 87.7° to 89.0°. It is immediately apparent that even for modest voltages of order a few hundred volts, substantial deflections of ~1° can be obtained. For the  $\theta_i = 87.7^\circ$  case, a line has been drawn to illustrate that the relationship at such angles is effectively linear

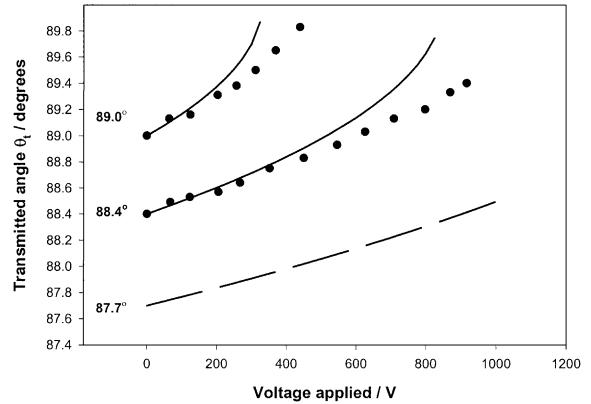


Fig. 4. Calculated transmitted angles  $\theta_t$  as a function of voltage applied for a range of values of  $\theta_i$  from 87.7° to 89.0°, a comparison is made with experimental results obtained for  $\theta_i = 88.4^\circ$  and  $89.0^\circ$ , using light from a 1.52 μm He–Ne laser.

for this voltage range. For the case of  $\theta_i = 88.4^\circ$ , a value we have investigated experimentally and is relatively easy to implement in a sample of interface length ~ 10 mm, a voltage of 300 V (corresponding to the normalised value of 1 kV mm<sup>-1</sup> across the 300 μm thick sample) produces an angular deflection of 0.39°. When compared to the value of angular deflection for the single prism deflector evaluated earlier, we see that this near TIR geometry is ~40 times higher in sensitivity.

Two further points to note in Fig. 4 are that we only present the deflection for one polarity of applied field. If the polarity of the applied field is reversed, there is the possibility of increasing the total deflection angle achievable, as the light will therefore be bent towards the normal in this case rather than towards the interface.

As the deflection angle increases, and TIR is approached, the transmitted intensity across the interface decreases. This is an important factor that must be addressed when considering the acceptable operating parameters of such a device. Fig. 5 shows the transmitted intensity calculated for the same range of applied field as shown in Fig. 4. While it is clear that for values of  $\theta_i > 89^\circ$ , the transmission falls rapidly as a function of applied field, for a value of  $\theta_i < 88^\circ$  the slope is small, and some degree of linearity again exists between transmission and applied field.

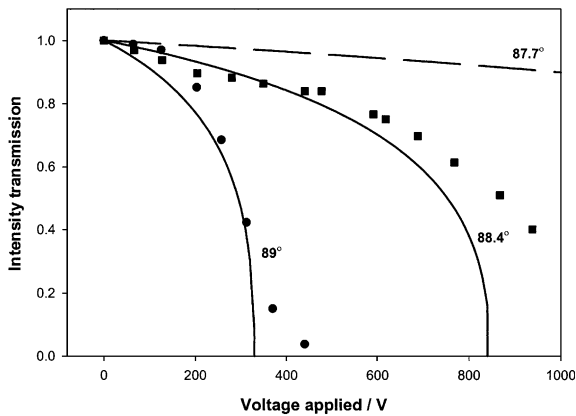


Fig. 5. Intensity transmission across the interface as a function of voltage applied, for a range of values of  $\theta_i$  from  $87.7^\circ$  to  $89.0^\circ$ , a comparison is made with experimental results obtained for  $\theta_i = 88.4^\circ$  and  $89.0^\circ$ , using light from a  $1.52 \mu\text{m}$  He–Ne laser.

A comparison of these results with those obtained experimentally using ‘s’ polarised light from an IR. He–Ne laser operating at  $1.523 \mu\text{m}$ , are represented by dots on the equivalent figure. It is seen that the overall shape is very similar to the theoretical plots, allowing for both the uncertainty of the *absolute* value of  $\theta_i$  which is difficult to measure precisely at such steep grazing incidence angles and carries an estimated uncertainty of order  $0.1\text{--}0.2^\circ$ , and also the fact that the interface is not straight at the better than  $0.1^\circ$  level. A final difference between the theoretical plots and the experimental data is that the beam is focussed to a waist at the middle point of the device, and hence some divergence, will occur in the wings of the Gaussian beam, which intersect the interface at a point other than the middle of the device. We are currently modelling this behaviour that will modify the shape of the plots obtained, rather than introduce the small noise we see in the measurement of both angle and transmitted power. We will shortly be fabricating such domain interfaces in stoichiometric rather than congruent  $\text{LiNbO}_3$  and we expect that the interface quality will be better.

### 3. Improvements to the device linearity

There is a final improvement that can be made to the performance of the device in terms of the

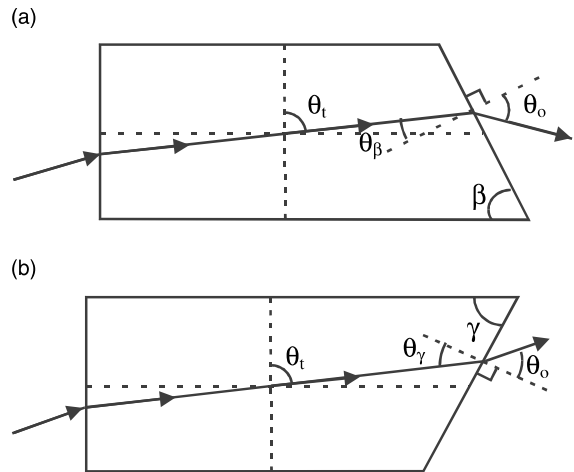


Fig. 6. Schematic of scanners with polished exit facets. The beam exits the rear face with angles of incidence  $\theta_\beta$  (a) and  $\theta_\gamma$  (b) respectively.

linearity and range of the deflection angle obtained, and which simultaneously flattens the transmitted intensity characteristics. Fig. 6 shows a simple modification to the output end of the sample, in which a facet is polished at an angle of  $\beta$  or  $\gamma$  respectively. The facet acts to magnify the angular deflection via the normal Snell law of refraction into a less dense medium, and if the angle is chosen appropriately, there is also a compensating behaviour for the previous transmission drop and the nonlinearity of angular deflection.

Fig. 7 illustrates this behaviour for a value of  $\theta_i = 87.75^\circ$  for a facet angled as shown in Fig. 6(a), this is represented by the solid line. In this geometry however, although the external angle of deflection is substantially increased when compared to that through an end face polished normally to the ray direction, the linearity is poor. Nevertheless, for  $\beta = 62.5^\circ$  a deflection of  $\sim 8^\circ$  is achievable for the voltage range between 0 and 1000 V. For the normalised value of  $1 \text{ kV mm}^{-1}$  an angular deflection of  $1.6^\circ$  is achieved compared to a value of  $0.5^\circ$  without the exit facet.

When the facet is angled the opposite way, as shown in Fig. 6(b), then the opportunity exists to simultaneously have a large deflection range, and good linearity of deflection and transmission as a function of voltage applied. Although the linearity

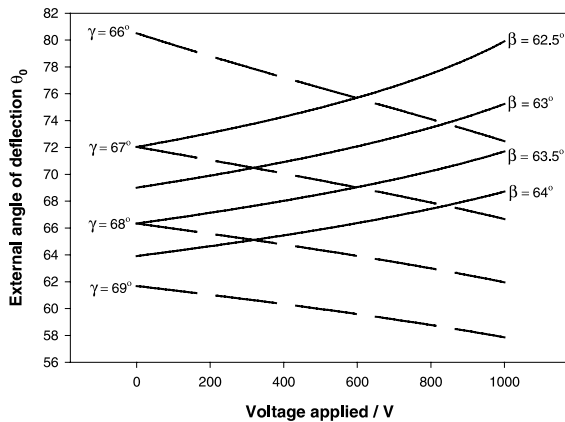


Fig. 7. External angle of deflection  $\theta_0$  as a function of voltage applied, for the arrangement of Fig. 6(a), for facet angles  $\beta$  between  $62.5^\circ$  and  $64.0^\circ$  (represented by the solid lines). The dashed lines represent the external angle of deflection  $\theta_0$ , for the arrangement of Fig. 6(b), for facet angles  $\gamma$  between  $66.0^\circ$  and  $69.0^\circ$ . The value of  $\theta_t$  for both cases is  $87.75^\circ$ .

of deflection is not an intrinsic necessity, and can be calibrated out, it is a desirable attribute if implementation is easy. The dashed line of Fig. 7 shows calculations for this oppositely angled facet. As  $\theta_t$  increases, the value of  $\theta_\gamma$  decreases, thereby reducing the Fresnel reflectivity from this angled facet and acting to compensate for the decreasing value of transmission across the interface. Fig. 7 show plots for facet angles spanning the range  $66\text{--}70^\circ$ . Fig. 8 presents a final comparison between a

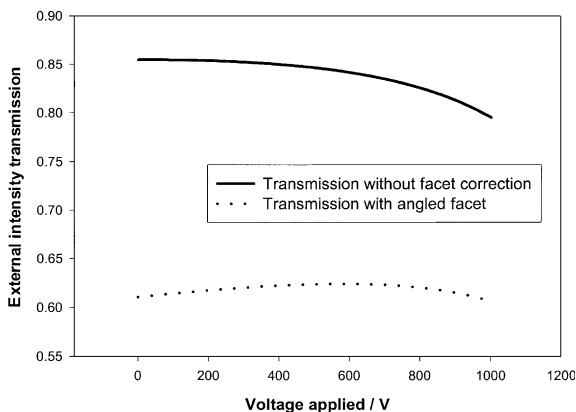


Fig. 8. Comparison between external intensity transmission with the facet as in Fig. 6(b) and without rear faceting, as a function of voltage applied.

facet angled at  $69^\circ$  and a facet polished at effectively normal incidence. Although greater Fresnel reflectivity invariably occurs for this ‘s’ polarised state at these angles, it is immediately apparent that the transmission reduction has been at least partially compensated. For this geometry ( $\theta_t = 87.75^\circ$ ), this compensation is at the expense of an overall reduction of  $\sim 27\%$  of the transmitted intensity.

#### 4. Conclusion

In conclusion we have presented a novel electro-optic beam deflector geometry, which permits a wide angular scan range, with simultaneous capability for good linearity of both deflection angle and transmission uniformity as a function of applied field. When compared to existing schemes for electro-optic scanning based on prisms, it is seen that this new geometry has a sensitivity that is between one and two orders of magnitude larger. We have shown that this geometry can function well as a beam deflector at the useful telecoms wavelength of  $1.52\ \mu\text{m}$ .

#### Acknowledgements

The authors are grateful to the Engineering and Physical Sciences Research Council (EPSRC) for funding for AJB and for research funding via grant no. GR/N00302.

#### References

- [1] J. Li, H.C. Cheng, M.J. Kawas, D.N. Lambeth, T.E. Schlesinger, D.D. Stancil, Electro-optic wafer beam deflector in  $\text{LiTaO}_3$ , *IEEE Photon. Technol. Lett.* 8 (1996) 1486–1488.
- [2] Q. Chen, Y. Chiu, D.N. Lambeth, T.E. Schlesinger, D.D. Stancil, Guided-wave electro-optic beam deflector using domain reversal in  $\text{LiTaO}_3$ , *J. Lightwave Technol.* (1994) 1401–1404.
- [3] K.T. Gahagan, V. Gopalan, J.M. Robinson, Q.X. Jia, T.E. Mitchell, M.J. Kawas, T.E. Schlesinger, D.D. Stancil, Integrated electro-optic lens/scanner in a single crystal  $\text{LiTaO}_3$ , *Appl. Opt.* 38 (1999) 1186–1190.
- [4] Y. Chiu, V. Gopalan, M.J. Kawas, T.E. Schlesinger, D.D. Stancil, Integrated optical device with second-harmonic

- generator, electro-optic lens, and integrated scanner in LiTaO<sub>3</sub>, *J. Lightwave Technol.* 17 (1999) 462–465.
- [5] K.S. Abedin, T. Tsuritani, M. Sato, H. Ito, K. Shimamura, T. Fukuda, Integrated electrooptic Q switching in a domain-inverted laser Nd:LiTaO<sub>3</sub>, *Opt. Letts.* 20 (1995) 1985–1987.
- [6] Y. Chiu, J. Zou, D.D. Stancil, T.E. Schlesinger, Shape-optimized electrooptic beam scanners: analysis, design, and simulation, *J. Lightwave Technol.* 17 (1999) 108–114.
- [7] E. Hecht, *Optics*, Addison-Wesley, Reading, MA, 1998.
- [8] A.J. Boyland, G.W. Ross, S. Mailis, P.G.R. Smith, R.W. Eason, Total internal reflection switching in electro-optically addressable domain-engineered LiNbO<sub>3</sub>, *Elec. Letts.* 7 (2001) 585–587.
- [9] M.J. Brinkman, A. Romanovsky, X. Saho, S.J. Field, D.A.G. Deacon, W.K. Bischel, Electro-optic switches in poled lithium niobate, *Cleo'96 Proceeding*, 1996.